Research Article

Increase in cation exchange capacity by the action of maize rhizosphere on Mg or Fe biotite-rich rocks[1]

Luise Lottici Krahl[2], Giuliano Marchi[3], Simone Patrícia Aranha Paz[4], Rômulo Simões Angélica[4], José Carlos Sousa-Silva[3], Leonardo Fonseca Valadares[5], Éder de Souza Martins[3]

ABSTRACT

The weathering of some silicate minerals in crushed rocks may occur in a few days of cropping and generate different physicochemical properties, with potential benefits to tropical soils. This study aimed to investigate the influence of maize (*Zea mays* L.) rhizosphere on the weathering products and on the cation exchange capacity of Mg-biotite from biotite schist and Fe-biotite from biotite syenite. An experiment was carried out in pots, so that plants and crushed rock materials could be evaluated during seven successive growth cycles. The nutrients iron and potassium were taken up from biotite schist and biotite syenite during cropping. The weathering of both biotites promoted by the rhizosphere caused mineralogical changes. The most expressive change in the X-ray diffraction patterns occurred in the < 53 μm particle size fraction; however, the 53-300 μm fractions also changed. The alteration in the Mg-biotite, which has a lower Fe/Mg relation in octahedral sites than the Fe-biotite, was responsible for the most expressive cation exchange capacity increase in the fractions < 300 μm. However, the Fe-biotite weathering process, which presents a higher Fe/Mg relation in octahedral sites, did not increase the cation exchange capacity.

KEYWORDS: *Zea mays* L., bioweathering, silicate agrominerals, potassium release, crushed rocks.

RESUMO

Aumento na capacidade de troca de cátions em rochas biotitas ricas em Mg ou Fe pela ação da rizosfera do milho

O intemperismo de alguns minerais silicáticos em rochas moídas pode ocorrer em alguns dias de cultivo e gerar diferentes propriedades físico-químicas, com benefícios potenciais a solos tropicais. Objetivou-se investigar a influência da rizosfera do milho (*Zea mays* L.) nos produtos do intemperismo e na capacidade de troca de cátions da biotita-Mg da biotita xisto e biotita-Fe da biotita sienito. Um experimento em vasos foi conduzido de forma que plantas e rochas moídas foram avaliadas por sete ciclos de cultivo sucessivos. Os nutrientes ferro e potássio foram adquiridos da biotita xisto e da biotita sienito durante o cultivo. O intemperismo das biotitas promovido pela rizosfera causou mudanças mineralógicas. A mudança mais expressiva nos padrões da difração de raios-X ocorreu na fração com partículas < 53 μm, mas as frações 53-300 μm também mudaram. A alteração na biotita-Mg, que possui menor relação Fe/Mg nos sítios octaedrais que a biotita-Fe, foi responsável pelo maior aumento na capacidade de troca de cátions nas frações < 300 μm. Entretanto, o processo de intemperismo da biotita-Fe, a qual apresenta alta relação Fe/Mg nos sítios octaedrais, não aumentou a capacidade de troca de cátions.

PALAVRAS-CHAVE: *Zea mays* L., biointemperismo, agrominerais silicáticos, liberação de potássio, rochas moídas.

INTRODUCTION

Selected crushed silicate rocks, used as agrominerals, may be regarded as a primary source of nutrients for plants, working as slow-release fertilizers (Li et al. 2015a, Manning et al. 2017). Macro and micronutrients required for plant growth are abundant in these minerals; however, the selection of sources for agricultural use does not depend only on the absolute nutrient content, but rather on the rate that minerals dissolve and on nutrients that become available for plants (Marchi et al. 2020).

Some previous studies have reported the ability of different silicate rocks to provide nutrients

[1] Received: Mar. 28, 2022. Accepted: July 27, 2022. Published: Sep. 13, 2022. DOI: 10.1590/1983-40632022v5272376.

[2] Universidade de Brasília, Faculdade UnB de Planaltina, Planaltina, DF, Brasil.
E-mail/ORCID: luisekrahl@yahoo.com.br/0000-0003-0622-8834.
[3] Empresa Brasileira de Pesquisa Agropecuária (Embrapa Cerrados), Planaltina, DF, Brasil.
E-mail/ORCID: giuliano.marchi@embrapa.br/0000-0002-2887-790X; jose.sousa-silva@embrapa.br/0000-0001-5648-6773, eder.martins@embrapa.br/0000-0003-2881-683X.
[4] Universidade Federal do Pará, Instituto de Geociências, Belém, PA, Brasil.
E-mail/ORCID: paz@ufpa.br/0000-0002-5880-7638, angelica@ufpa.br/0000-0002-3026-5523.
[5] Empresa Brasileira de Pesquisa Agropecuária (Embrapa Agroenergia), Brasília, DF, Brasil.
E-mail/ORCID: leonardo.valadares@embrapa.br/0000-0001-6668-1433.

to plants in a short time scale, especially on the release of K (Li et al. 2015a, Manning et al. 2017). Besides, a significant proportion of K required for plant growth can be extracted from K-rich minerals available from silicate rocks containing biotite and their weathering products (Norouzi & Khademi 2010, Mohammed et al. 2014, Manning et al. 2017).

Weathering rates during mica weathering vary according to its mineralogy. The release of cations from these trioctahedral micas during the incongruent dissolution may lead to the formation of secondary minerals containing 2:1 layers, amorphous phases and low crystallinity minerals (Yu et al. 2018, Wu et al. 2021). During the beginning of the natural weathering process of biotite minerals, an expanded interstratified biotite-vermiculite (hydrobiotite) is formed. Hydrobiotite presents a large peak in X-ray analysis, ranging from 10 to ~24 Å, due to the interlayer expansion on the edge of biotite layers. It is expected a buildup of a peak at 14 Å, along the time, reflecting the presence of vermiculite minerals (Murakami et al. 2003). Both hydrobiotite and vermiculite may contribute to the increase of soil cation exchange capacity (Churchman & Lowe 2012). However, the biotite chemical composition, especially its Fe and Mg contents, as well as the elements substitution in the octahedral and tetrahedral silicate sheets (e.g., Si^{4+} by Al^{3+} and Fe^{3+} in tetrahedral sites or Al^{3+} by Mg^{2+} in octahedral sites), lead to different weathering rates (Murakami et al. 2003).

Biotite-bearing rocks, like some schists and syenites, are widely available in tropical environments. These rocks may present a relatively fast dissolution in agroecosystems, being able to release nutrients to plants (Li et al. 2015a, Manning et al. 2017). Yet, the weathering rate of biotite-rich rocks, as well as physicochemical properties of their products after weathering, under the influence of the rhizosphere, have not been thoroughly described.

A full understanding of these processes is important, as they are linked to the rate/amount of nutrients which may be released in soils after these rocks are used as agrominerals. During the incongruent dissolution of rocks, new particles are formed. Particles presenting permanent negative charges can improve soil properties, especially for highly weathered, low cation exchange capacity soils, such as tropical Oxisols. Given that, there is a lack of information concerning secondary minerals forming rates (Wu et al. 2021), and the resulting cation exchange capacity (CEC) after bioweathering in the rhizosphere.

Thus, this study aimed to evaluate the bioweathering of Fe and Mg biotites promoted on the maize rhizosphere, evaluating the rates of elements offtake, appearance of secondary minerals and the CEC increase rate of the weathered rocks.

MATERIAL AND METHODS

Biotite schist (BSC) was collected from residue piles in quarries located in Abadiânia, Goiás state, Brazil (Navarro et al. 2013), while biotite syenite (BSY) was collected in the Ceraíma massif, southeastern of the Bahia state, Brazil (Cruz et al. 2016). Samples (150 kg of each rock) were air-dried and homogenized using the cone-and-quartering reduction method, forming the bulk sample.

Pure rock samples (BSC and BSY) were placed into 500 mL pots. Two plants of maize (*Zea mays* L.) per pot were grown in sets of three pots, repeated for seven growth cycles, totaling 42 pots (21 pots of each rock). Seven extra pots of each rock without plants were prepared as a control treatment. Each growth cycle took 45 days. The experiment began in April 2016 and was concluded, after 7 cycles of 45 days, in January 2017.

The pots were watered to 70 % of the water pot capacity, previously calculated from uncropped container medium, and fertilized with nutrient solution (92.76 mg pot^{-1} of $NH_4H_2PO_4$) on the 15th and 30th days of growth of each cycle.

At the end of each cycle, whole plants from all pots were harvested. The rock material content from one set of three pots, plus one control pot, previously grown with plants, were collected for further analysis. The remaining sets were re-sown for a new growth cycle. As the experiment was designed as a destructive testing, the last cycle had only four pots for each rock, including the control pot.

The harvested plants were oven dried at 65 ºC, for 72 hours. Potassium, iron and magnesium in dry biomass (total dry mass comprising leaves, shoots and roots) were extracted by HNO_3:$HClO_4$, in a digestion block (Embrapa 2017), and determined by inductively coupled plasma optical emission spectrometry (ICP-OES).

After each harvest cycle, the content of the respective set of pots was prepared for pH analysis

and fractionation. The pH of the bulk samples was determined one hour after mixing the sample in water at a 1:2.5 ratio. After that, bulk samples were wet sieved to separate the material in four size fractions: < 53 µm, 53-300 µm, 300-1,000 µm and > 1,000 µm (Table 1), so that to evaluate only the crystalline minerals.

Electron probe microanalyses (EPMA) were carried out to identify the biotite mineral within the samples with a JEOL (model Superprobe JXA-8230), coupled with 5 spectrometers and one energy dispersive spectrometer (EDS) detector, operating with 10 nA of current and 15 kV. The acquisition time was 10 seconds by step and 5 seconds at the background, and the beam diameter was 1 µm. The instrument was calibrated using natural and synthetic primary standards and the resulting data processed to calculate the structural formulas of the mineral phases. The analyses involved a total of 24 biotite crystals (10 of BSC and 14 of BSY).

Total chemical analyses of the BSC and BSY samples were carried out using wavelength dispersive X-ray fluorescence (XRF) spectroscopy and ICP-OES, following a multi-acid solution digestion (Table 2). Major elements were determined on fused glass discs (40 mm diameter) prepared from 0.8 g of sample powder mixed with 4.5 g of lithium tetraborate flux and fused in Pt-5 % Au crucibles at 1,120 ºC (SGS Geosol Laboratórios Ltda). The multi-acid solution method consisted of digesting 500 mg of sample in 10:15:10:5 mL of $HCl:HNO_3:HF:HClO_4$, respectively, and afterward minor elements were determined by ICP-OES (SGS Geosol Laboratórios Ltda). In order to determine the loss on ignition, the samples were heated overnight at 105 ºC, to remove water, and the weight loss was measured after the calcination of samples at 1,000 ºC for approximately 2 hours.

The mineralogical composition of the BSC and BSY fractions before and after every crop cycle were analyzed by X-ray diffraction analysis (XRD), employing a PANalytical Empyrean (PW3050/60) diffractometer, using the powder method in the range of 5 º < 2θ < 75 º. CoKα radiation (40 kV; 40 mA) was applied, and the 2θ scanning speed was set at 0.02 º s^{-1}. The data was acquired using the X'Pert Data Collector 4.0 software and treated on the X'Pert HighScore 3.0 (PANalytical). Minerals were identified by comparing the obtained diffractogram with the ICDD-PDF (International Center for Diffraction Data) database.

The transformation rate of biotite into hydrobiotite for both the BSC and BSY was estimated

Table 1. Particle-size distribution of crushed rock powders used in the experiment.

Sample	Particle-size distribution (µm)				Total (g pot^{-1})
	< 53	53-300	300-1,000	> 1,000-2,000	
	%				
Biotite schist	21.1	17.4	2.4	59.1	546.82
Biotite syenite	11.9	23.2	29.6	35.3	681.02

Table 2. Chemical composition of the biotite schist and biotite syenite powder (bulk sample and fractions) determined by XRF and ICP-OES[a].

Sample	Fraction (µm)	SiO_2	Al_2O_3	Fe_2O_3	CaO	MgO	TiO_2	P_2O_5	Na_2O	K_2O	MnO	BaO	Cr_2O_3	Cu	Mo	Zn	LOI[b]	Total
		%												mg kg^{-1}				%
Biotite schist	< 53	59.6	16.1	8.06	2.31	3.84	1.08	0.29	2.57	2.61	0.06	0.06	0.02	104	< 3	104	2.18	96.60
	53-300	59.7	19.0	7.74	0.87	3.68	0.57	0.15	1.84	4.14	0.05	0.11	0.02	35	< 3	35	2.72	97.87
	300-1,000	67.1	14.4	6.49	1.31	2.38	0.94	0.13	2.23	2.38	0.11	0.05	0.01	73	< 3	73	1.59	97.53
	> 1,000	66.4	15.1	7.22	1.54	2.55	0.83	0.17	2.21	2.53	0.16	0.06	0.01	53	< 3	53	1.50	98.78
	Bulk sample[c]	62.6	16.8	7.80	1.44	3.20	0.86	0.20	1.93	3.19	0.12	0.07	0.02	49	< 3	49	2.17	98.23
Biotite syenite	< 53	53.4	14.6	10.50	3.38	2.16	2.31	0.61	1.49	9.36	0.17	0.58	0.01	88	< 3	88	1.28	98.57
	53-300	53.7	14.9	11.10	2.69	2.14	2.32	0.38	1.19	10.70	0.14	0.58	0.01	46	< 3	46	0.37	99.85
	300-1,000	57.3	16.1	8.51	1.63	1.72	1.29	0.19	1.15	11.90	0.11	0.58	< 0.01	35	< 3	35	0.36	100.48
	> 1,000	57.6	16.0	7.41	1.89	1.54	1.26	0.24	1.38	11.80	0.11	0.60	< 0.01	32	< 3	32	0.29	99.83
	Bulk sample[c]	55.9	16.0	8.16	2.00	1.70	1.49	0.24	1.19	11.30	0.11	0.57	< 0.01	31	< 3	31	0.49	98.66

[a] SGS Geosol Laboratórios Ltda; [b] loss on ignition; [c] original sample.

by XRD reflection areas, using the Equation 1: Hydrobiotite:biotite ratio per cycle (%) = [(hydrobiotite reflection area)/(hydrobiotite reflection area + biotite reflection area)] x 100. The reflection area was used to estimate a ratio for the biotite:muscovite ratio from the BSC by the Equation 2: Biotite:muscovite ratio per cycle (%) = [(biotite reflection area)/(biotite reflection area + muscovite reflection area)] x 100.

Rietveld refinement was performed using the High Score Plus software (Malvern Panalytical, version 4.7) for quantitative determination of the mineralogical composition in each size fraction of the BSC and BSY samples (Table 3). The structural models (CIF files) for the identified mineral phases were obtained from the ICSD database. The traditional sequence for such refinements is as it follows: scale factor and background, using a polynomial function, besides unit cell parameters for all phases. The W parameter of the Caglioti equation is refined only for the major phases, followed by V and U. Chlorites and micas exhibit a strong preferred orientation and the (00l) direction must be refined as the same for the (100) plane of the feldspars (microcline and albite). Atomic positions were not refined.

The morphology of the samples was examined by scanning electron microscopy (SEM) on a Zeiss SIGMA HV field emission microscope at 5 kV, using the InLens detector. The samples were pulverized over conductive double-face carbon tape fixed on SEM stubs. A thin conductive layer of gold (10 nm) was deposited over the samples using the Q150T-ES sputter (Quorum Technologies).

Samples of BSC and BSY after each growth cycle were analyzed for cation exchange capacity (CEC) using the BS-ISO 11260 method (BSIOS 2011). The Texas Montmorillonite (STx-1), Gonzales county, Texas, USA, was used as a standard reference for the measured CEC. The amount of STx-1 used in the CEC analysis was 1 g. Values for CEC of the STx-1 (average ± standard deviation, n = 12) were 66.8 ± 4.05 $cmol_c\ kg^{-1}$. The CEC analysis was performed in non-weathered, original BSC and BSY samples, as a reference, and in samples obtained after each growth cycle, which showed evidence of hydrobiotite formation in X-ray diffractograms.

Statistical analyses were performed using the Sigma Plot 12.0 software (Sigma Plot Software, San Jose, California, USA). Equations were selected according to the analysis of variance and, thereafter, were tested for normality (Shapiro & Wilk 1965) and equal variance test (homoscedasticity) (O'Neill & Mathews 2000), considering p-values < 0.05 significant.

RESULTS AND DISCUSSION

The chemical and mineralogical composition of bulk samples and fractions (Tables 1, 2 and 3) showed the presence of biotite in both the BSC and BSY, which is the main active mineral likely to weather, releasing nutrients such as K, Ca, Mg, Fe and Mn (Table 3).

The biotite analyzed in both rocks varied as to MgO and FeO contents by EPMA. The biotite within the BSC samples presented higher MgO and Al_2O_3 contents in octahedral sites (referred henceforth as Mg-biotite). The Mg-biotite [chemical composition: $K_{0.817}\,Ba_{0.005}\,(Mg_{1.198}\,Fe_{1.157}\,Al_{0.415}\,Ti_{0.088})\,(Si_{2.845}\,Al_{1.154}\,O_{11})\,(OH_{1.97}\,F_{0.02}\,Cl_{0.001})$] was, therefore, in the annite, siderophyllite and phlogopite interface (Tischendorf et al. 2007). The biotite within the BSY samples was classified as annite (Tischendorf et al. 2007), which is a Fe-biotite [composition: $K_{0.805}\,Ba_{0.022}\,Na_{0.011}\,(Fe_{1.55}\,Mg_{0.785}\,Ti_{0.168}\,Al_{0.255}\,Mn_{0.01})\,(Si_{2.963}\,Al_{1.036}\,O_{11})\,(OH_{1.949}\,F_{0.045}\,Cl_{0.005})$].

The pH of the bulk sample, measured after each cycle, decreased linearly after each growth

Table 3. Mineralogical composition of biotite schist and biotite syenite powder (bulk samples and fractions) used in the experiment.

Fraction (μm)	Biotite schist						Biotite syenite				
	Quartz	Albite	Biotite	Muscovite	Chlorite	Clinopyroxene	K-feldspar[b]	Albite	Biotite	Amphibole	Clinopyroxene
< 53	30.8	27.5	9.3	18.6	11.7	2.0	60.3	13.9	10.7	1.9	13.2
53-300	33.4	22.2	10.3	22.5	10.5	1.1	52.5	11.0	22.5	4.4	9.4
300-1,000	38.7	20.7	7.5	17.0	14.4	1.6	55.2	13.7	15.5	5.0	10.7
> 1,000	36.0	24.9	9.2	15.4	13.2	1.3	64.8	15.7	10.1	2.4	7.0
Bulk sample[a]	35.7	22.1	11.2	17.9	11.3	1.7	58.1	9.3	15.4	3.6	13.5

[a] Original sample; [b] orthoclase and microcline.

cycle [Equation 3: $pH_{biotite\ schist}$ = 7.49** - 0.22** (cycle), R^2 = 0.91; and Equation 4: $pH_{biotite\ syenite}$ = 7.93** - 0.36** (cycle), R^2 = 0.88]. The pH of the control samples did not change significantly (standard deviation = 8.0, 0.2, and 7.8, 0.2, respectively for BSC and BSY; ** $p < 0.01$ along the 7 cycles). The pH decrease was, therefore, promoted through the rhizosphere of plants during weathering.

The biotite weathering, at nearly neutral pH, involves oxidation of structural Fe(II) and exchange of interlayer K for ions in the external solution, while at acidic pH it proceeds through a near-congruent dissolution (Ryu et al. 2016).

In the course of the growth cycles, the maize plants showed differences in potassium offtake according to the substrate and crop cycle. The accumulated potassium offtake by plants grown successively during 315 days in the BSC was 0.704 g pot^{-1}, and, in the BSY, it was 0.431 g pot^{-1}. The K offtake by plants was higher in the first cycle for both rocks, and then it decreased along the cycles according to the Equation 5 [$K_{offtake\_biotite\ schist\ (g\ per\ pot)}$ = 0.15** - 0.04** ln(cycle), R^2 = 0.91] and 6 [$K_{offtake\_biotite\ syenite\ (g\ per\ pot)}$ = 0.09** - 0.007*(cycle), R^2 = 0.73] (** $p < 0.01$; * $p < 0.05$).

The K uptake by plants was specific for each rock; however, it was not related to the total concentration of this element in the rocks. Although the total K and biotite contents in the BSY bulk sample were higher than in the BSC (Tables 2 and 3), the total K offtake was lower in plants grown in the BSY. Therefore, biotite in the BSC was more susceptible to weathering than the K-feldspars and biotite found in the BSY.

After 315 days of successive growth, the greatest XRD pattern changes occurred in the finer size fraction (< 53 µm; Figure 1). The formation of interstratified mica-vermiculite, even as to the coarser particle size fraction (53-300 µm), was also observed for the BSC and BSY (Figure 1). This upshot shows that coarser particles are not chemically inert in a short time scale.

The practical use of this information is that great part of the BSC and BSY applied to agricultural soils (> 80 % w/w) should be milled < 300 µm. The availability of K from K-rich silicate minerals may be substantially altered by milling, which can transform minerals structural K into available forms and increase the percentage of finer fractions in the milled material (Madaras et al. 2013).

The nutrient release from crushed rocks is dependent on the grain size (Bray et al. 2015) and on the density of surface defects of the material. Adjusting the silicate rock powders size for agricultural use increases its rates of dissolution and nutrient availability (Harley & Gilkes 2000). Thus, the reactivity of BSC and BSY will be higher in the finer fractions, preferentially in those < 53 µm.

The X-ray diffraction analysis pattern of particles smaller than 53 µm of BSC and BSY detected mineralogical transformations occurring right after the first 45-day-cycle (Figure 2). The XRD pattern of the < 53 µm collected from pots without plants (control samples) after 315 days of incubation were like the XRD results of the original material (before the experiment) for both the BSC and BSY. There was no evidence of weathering on the control samples, and, for this reason, the maize rhizosphere

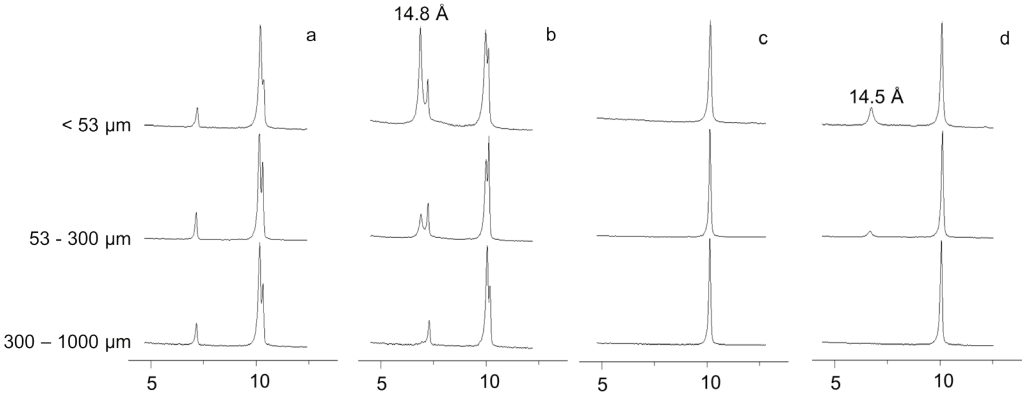

Figure 1. X-ray diffraction patterns of three size particles of biotite schist original samples (a), biotite schist samples after 315 days of interaction with maize rhizosphere (b), biotite syenite original samples (c) and biotite syenite samples after 315 days of interaction with maize rhizosphere (d).

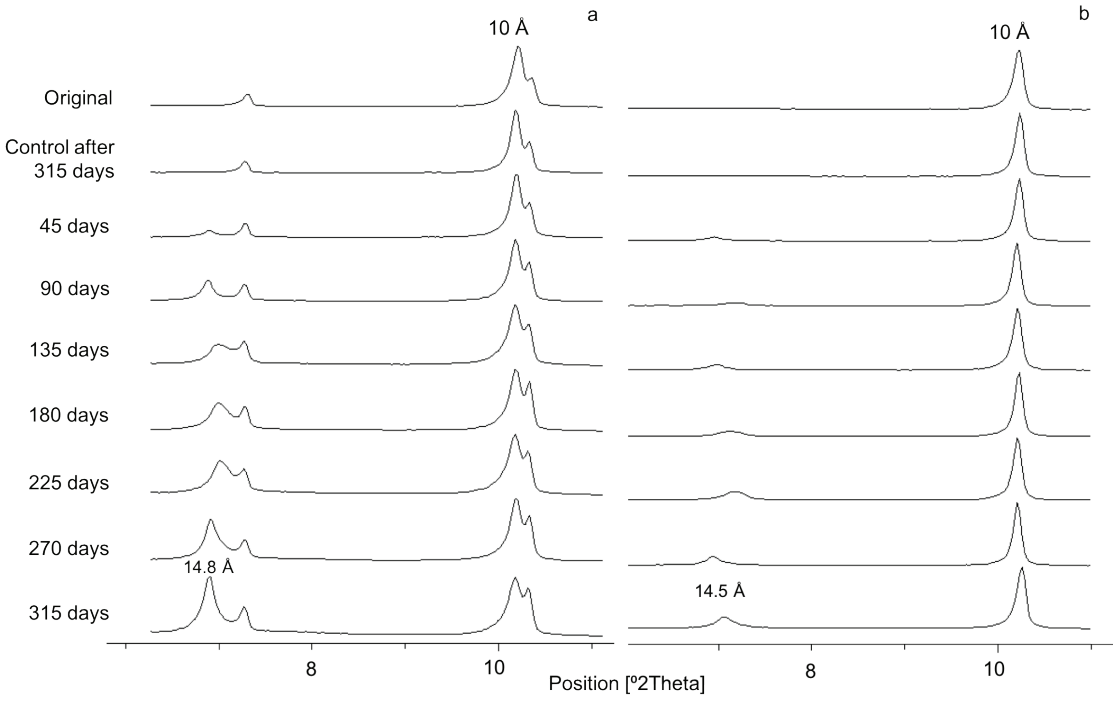

Figure 2. X-ray diffraction patterns of < 53 µm size particles of biotite schist (a) and biotite syenite (b) after interaction with maize rhizosphere.

was the responsible for the weathering observed in the rock materials.

The XRD pattern from the BSC after each of the seven cycles (totaling 315 days) showed a progressive process of vermiculitization (Figure 2). The edges of the Mg-biotite grains expanded and, consequently, characteristic broad reflections for the new-formed hydrous mica were detected. Hydrobiotite - a precursor of vermiculite - is a mica that has gained water by losing a part of its K content. The hydrobiotite reflection at 14.8 Å emerged gradually, as roots extracted K from biotite interlayers. Mohammed et al. (2014) classified a corresponding appearance of the reflection at 14.8 Å in weathered biotite as a clear, defined, 002 vermiculite reflection.

A reflection at 14.5 Å in BSY indicated the hydrobiotite formation from the weathering of Fe-biotite (Figure 2). Norouzi & Khademi (2010) found the same peak reflection studying pure biotite weathered in the rhizosphere of alfalfa for 90 days. Those authors interpreted the reflections from the (001) planes as a typical vermiculite. Although the BSY was mostly constituted by a K-feldspar, the change in the XRD pattern was attributed only to the biotite, as it was a short experiment. Feldspars are more resistant to weather than biotite and kaolinite (Banfield & Eggleton 1990). A stable weathering product of feldspars was not identified in the XRD patterns observed.

The X-ray diffraction analysis of biotite and hydrobiotite reflection areas were used to estimate their relative percentages over time (Figures 3 and 4). The decrease in the biotite reflection area was related to the formation of hydrobiotite in the BSC along the time (Figure 3a; Equation 1). Thus, the hydrobiotite formation rate was negatively correlated with biotite on the < 53 µm size fractions (Pearson's correlation, $r = -0.88$; $p < 0.05$). This result indicated that the incongruent dissolution of Mg-biotite was the source for the hydrobiotite formation in the BSC samples.

The dissolution of the biotite in the BSC samples was estimated using muscovite [$KAl_2(AlSi_3O_{10})(OH,F,Cl)_2$] as an internal standard (Figure 4; Equation 2). Biotite, like muscovite, is a K-bearing 2:1 phyllosilicate; however, muscovite has a higher Al content than biotite, thus presenting a high resistance to weathering. The internal standard for the BSY, on the other hand, a K-feldspar (a high resistant mineral), did not allow correlating the biotite and hydrobiotite ratios. Therefore, the dissolution rate of biotite in the BSY samples was not estimated.

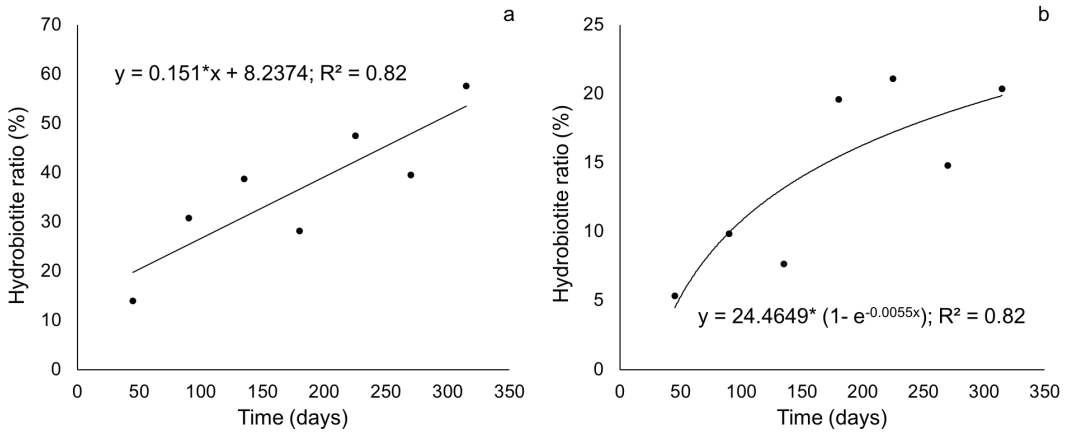

Figure 3. Hydrobiotite formation *versus* time. a) Biotite schist; b) biotite syenite.

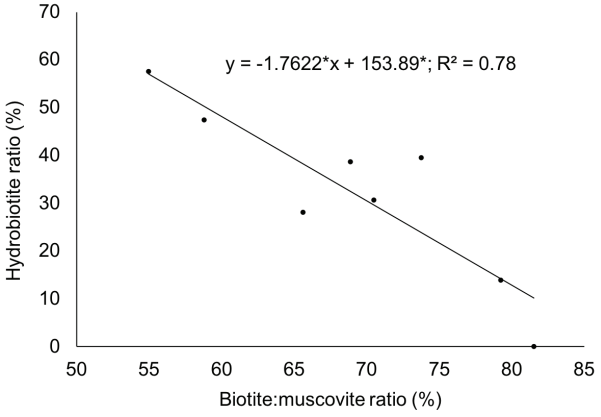

Figure 4. Relationship between biotite intensity XRD reflections and hydrobiotite formation in biotite schist.

The formation of hydrobiotite in the BSY samples was slower than in the BSC. The hydrobiotite formation was relatively faster in the initial crop cycles, but slowed down during the experiment (Figure 3b; Equation 1). Magnesium and Fe(II) contents on the biotite structure of the BSY, comprising a higher proportion of Fe/Mg in the octahedral site than for the BSC, may explain the slow pace of hydrobiotite formation rate. Plants accumulated 0.052 and 0.041 mg of Mg pot^{-1}, and 0.07 and 0.12 mg of Fe pot^{-1}, after 315 days, for the BSC and BSY, respectively. The variations in Fe and Mg contents and the substitution rate of elements in the octahedral and tetrahedral sheets lead to differences in the weathering rate of biotite minerals (Murakami et al. 2003, Madaras et al. 2013, Li et al. 2015b). Therefore, plants may have uptake Mg and Fe in different rates from BSC and BSY. The uptake rates concerning these two elements were related to dissolution kinetics of each biotite type, resulting in a differentiated dissolution and selective uptake of chemical elements according to the leachability of K from each silicate mineral (Wu et al. 2021).

The oxidation of octahedral Fe in biotite may be an important mechanism in the mineral structure that prevents the release of the interlayered K (Murakami et al. 2003). Structural Fe can stabilize or destabilize the K of the interlayer, depending on whether oxidation leads to release of Fe atoms from the octahedral sheet (Thompson & Ukrainczyk 2002). The oxidation of structural Fe(II) in octahedral sheets of micas may lead to interlayer expansion and K release. Conversely, the reduction of structural Fe(III) in the expanded 2:1 layer may lead to interlayer collapse and K fixation (Scott & Amonette 1988).

As the weathering proceeds, Fe-biotite, such as the one found in the BSY, becomes more stable and the weathering process slows down (Gilkes et al. 1972). As a matter of fact, initially, Fe(II) leaves the mineral structure and oxidizes to Fe(III). After this stage, the biotite-weathering rate decreases, exactly as occurred in the present experiment for the BSY samples (Figure 3). The difference in OH orientation has also been cited by Gilkes et al. (1972; 1973) as the cause of higher potassium retention in Fe-biotites after structural Fe(II) oxidation.

The Fe(II) oxidation excess (high Fe/Mg in biotite octahedral sites), such as for the BSY, decreases the weathering processes. However, a higher Mg content in the biotite composition accelerates the alteration that leads to vermiculite, as discussed by Murakami et al. (2003). Those authors

pointed out that the vermiculite formation via layer-by-layer transformation occurs even in the early stage of dissolution for Mg-biotite and phlogopite, nevertheless this process does not occur for Fe-biotite.

Even though the XRD analysis of both kinds of biotite showed that they dissolve incongruently throughout the experiment, forming hydrobiotite, a detailed observation of grain surfaces by SEM (Figure 5) supports the idea that fine-grained particles of biotite experienced a congruent dissolution, similarly to that which was demonstrated by Manning et al. (2017). After seven cycles, the surfaces of biotite grains from control samples (without plants) from both the BSC and BSY were covered with fine particles. On the other hand, on the surfaces of the biotite particles, which were submitted to the growth of plants during seven cycles, a reduction in the quantity of fine particles covering them was observed.

Coarser fractions of the BSY formed hydrobiotite after the seven growth cycles (Figure 1), and the < 53 μm fraction did not have its CEC modified along the experiment (CEC = 3.73 ± 0.93 $cmol_c$ kg^{-1}, n = 24, in seven cycles), when compared to the reference (original, not weathered BSY), not justifying further analysis of the BSY coarser fractions.

This lack of change in the CEC of the weathered BSY samples may be explained by the findings of Murakami et al. (2003), studying the dissolution of biotite in laboratory experiments. According to their studies, the solution was supersaturated with Fe and Al oxide-hydroxides very early. Iron is probably in the amorphous form and dispersed as fine-grained microcrystalline oxides on the surface and edges of oxidized biotite. In oxidizing conditions, reduced iron released from the mineral matrix, if not absorbed by plant roots, rapidly precipitates as amorphous Fe(III) hydroxides (Wu et al. 2021). The Fe precipitation on the surface of transforming minerals probably plays a role in delaying the weathering process and blocking charged sites formed on mineral surfaces (Bray et al. 2015).

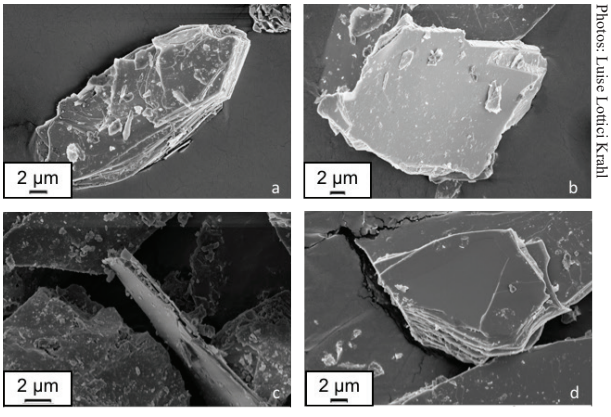

Figure 5. Scanning electron microscopy (SEM) images of biotite grains from maize growth experiments: biotite surface without plant growth (a) and after plant growth (b) on biotite schist; and biotite surface without plant growth (c) and after plant growth (d) on biotite syenite.

Charge properties of BSY, therefore, may have been altered after Fe oxides were formed in its surface (Scott & Amonette 1988). However, the wet sieving for the separation of the material allowed the evaluation of crystalline minerals, but not the newly formed low-crystalline minerals. Numerous new Fe-Si-rich amorphous phases (Fe short-range-ordered) minerals were neoformed in biotite samples after root interactions, according to Wu et al. (2021), as a result of co-precipitation of dissolved Fe(III) on mineral surfaces. Santos et al. (2021), working with the same source of BSY mixed in an Oxisol, found, after 45 days of maize growth, an increase in CEC from 2.6 to 3.0 $cmol_c$ kg^{-1}, indicating that, in soils, the co-precipitation of dissolved Fe(III) may be distributed over other particles, and did not hamper charge formation.

Nevertheless, < 53 μm and 53-300 μm fractions from the BSC showed hydrobiotite in the XRD patterns (Figure 1) and were analyzed for CEC. Along the growth cycles, the BSC showed a progressive increase in CEC (Figure 6). The CEC on the < 53 μm and 53-300 μm fractions increased along the experiments, respectively from 1.48 and 2.77 $cmol_c$ kg^{-1} to 8.91 and to 7.13 $cmol_c$ kg^{-1}, after 315 days of continuous growth.

The cation exchange capacity on the fraction < 53 μm and hydrobiotite formation rate were both positively correlated (Pearson's correlation, r= 0.92, $p < 0.05$; Figures 3a and 6). The slope of the CEC equations for each fraction is close to each other, thus the rate of CEC increase is similar for the two fractions under the action of the rhizosphere. The slope of the straight line formed with the CEC data along the growth cycles also suggests that higher values of CEC would be attained, granted that more cycles were provided.

The CEC presented in the < 300 μm fractions after the seven growth cycles suggests that the Mg-biotite has the potential to increase the CEC of soils

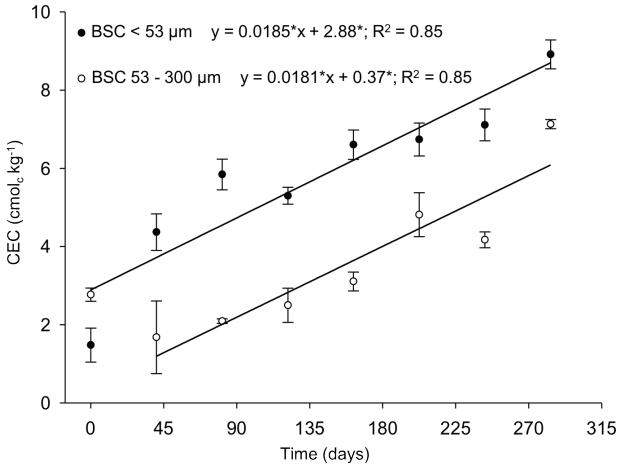

Figure 6. Cation exchange capacity (CEC) of < 53 and 53-300 µm size particles of biotite schist for 315 days (7 cycles) of interaction with maize rhizosphere.

with very low CEC, but it may only be recommended for agricultural use after increases in soil quality are thoroughly assured. As a parameter, highly weathered soils, as Oxisols, are characterized by relatively low $CEC_{pH\ 7.0}$ values [7.6 ± 5.9 cmol$_c$ kg^{-1} (Essington 2003); 7.1 ± 4.0 cmol$_c$ kg^{-1}, n = 23 (Marchi et al. 2015), for representative Oxisols of the Brazilian Cerrado]. The powder rocks BSC and BSY may weather in a diverse rate after applied and mixed to agricultural soils, because, in soils, the weathering rate decreases caused by the precipitation of Fe(III) in excess on Fe-biotite particle surfaces may not happen. In fact, the rock materials would be under intense exposition to other conditions than the observed in the present study.

CONCLUSIONS

1. There was bioweathering on the biotite-rich rock materials in a period as short as 45 days;
2. The initial release of K occurred by congruent dissolution from finer particles. The weathering of minerals also happened incongruently. An interstratified biotite-vermiculite (hydrobiotite) in both the Fe and Mg biotites was formed;
3. The Mg-biotite forms hydrobiotite, increasing its overall cation exchange capacity;
4. The Fe(II) oxidation in Fe-biotite from biotite syenite generates a stable environment, preventing both further releases of K and increases in the cation exchange capacity.

REFERENCES

BANFIELD, J. F.; EGGLETON, R. A. Analytical transmission electron microscope studies of plagioclase, muscovite, and K-feldspar weathering. *Clays and Clay Minerals*, v. 38, n. 1, p. 77-89, 1990.

BRAY, A. W.; OELKERS, E. H.; BONNEVILLE, S.; WOLFF-BOENISCH, D.; POTTS, N. J.; FONES, G.; BENNING, L. G. The effect of pH, grain size, and organic ligands on biotite weathering rates. *Geochimica et Cosmochimica Acta*, v. 164, n. 1, p. 127-145, 2015.

BRITSH STANDARD INTERNATIONAL ORGANIZATION FOR STANDARDIZATION (BSIOS). *BS-ISO 11260*: soil quality: determination of effective cation exchange capacity and base saturation level using barium chloride solution. Brussels: International Organization for Standardization, 2011.

CHURCHMAN, G. J.; LOWE, D. J. Alteration, formation, and occurrence of minerals in soils. *In*: HUANG, P. M.; LI, Y., SUMNER, M. E. (ed.). *Handbook of soil sciences*. 2. ed. Boca Raton: CRC Press, 2012.

CRUZ, S. C. P.; BARBOSA, J. S. F.; PINTO, M. S.; PEUCAT, J. J.; PAQUETTE, J. L.; SOUZA, J. S. de; MARTINS, V. D.; CHEMALE, F.; CARNEIRO, M. A. The siderian-orosirian magmatism in the Gaviao Paleoplate, Brazil: U-Pb geochronology, geochemistry and tectonic implications. *Journal of South American Earth Sciences*, v. 69, n. 1, p. 43-79, 2016.

EMPRESA BRASILEIRA DE PESQUISA AGROPECUÁRIA (Embrapa). *Manual de métodos de análise de solo*. 3. ed. Rio de Janeiro: Centro Nacional de Pesquisa de Solos, 2017.

ESSINGTON, M. E. *Soil and water chemistry*: an integrative approach. 2. ed. Boca Raton: CRC Press, 2003.

GILKES, R. J.; YOUNG, R. C.; QUIRK, J. P. Artificial weathering of oxidized biotite: I. Potassium removal by sodium chloride and sodium tetraphenylboron solutions. *Soil Science Society of America Journal*, v. 37, n. 1, p. 25-28, 1973.

GILKES, R. J.; YOUNG, R. C.; QUIRK, J. P. The oxidation of octahedral iron in biotite. *Clays and Clay Minerals*, v. 20, n. 5, p. 303-315, 1972.

HARLEY, A. D.; GILKES, R. J. Factors influencing the release of plant nutrient elements from silicate rock powders: a geochemical overview. *Nutrient Cycling and Agroecosystems*, v. 56, n. 1, p. 11-36, 2000.

LI, T.; WANG, H.; WANG, J.; ZHOU, Z.; ZHOU, J. Exploring the potential of phyllosilicate minerals as potassium fertilizers using sodium tetraphenylboron and intensive cropping with perennial ryegrass. *Scientific Reports*, v. 5, n. 1, p. 1-7, 2015a.

LI, T.; WANGA, H.; ZHOU, Z.; CHEN, X.; ZHOU, J. A nano-scale study of the mechanisms of non-exchangeable potassium release from micas. *Applied Clay Sciences*, v. 118, n. 1, p. 131-137, 2015b.

MADARAS, M.; MAYEROVÁ, M.; KULHÁNEK, M.; KOUBOVÁ, M.; FALTUS, M. Waste silicate minerals as potassium sources: a greenhouse study on spring barley. *Archives of Agronomy and Soil Science*, v. 59, n. 5, p. 671-683, 2013.

MANNING, D. A. C.; BAPTISTA, J.; LIMON, M. S.; BRANDT, K. Testing the ability of plants to access potassium from framework silicate minerals. *Science of the Total Environment,* v. 574, n. 1, p. 476-481, 2017.

MARCHI, G.; GUELFI-SILVA, D. R.; MALAQUIAS, J. V.; GUILHERME, L. R. G.; SPEHAR, C. R.; MARTINS, E. D. S. Solubility and availability of micronutrients extracted from silicate agrominerals. *Pesquisa Agropecuária Brasileira*, v. 55, e00807, 2020.

MARCHI, G.; VILAR, C. C.; O'CONNOR, G.; SILVA, M. L. N. Surface complexation modeling in variable charge soils: charge characterization by potentiometric titration. *Revista Brasileira de Ciência do Solo*, v. 39, n. 5, p. 1387-1394, 2015.

MOHAMMED, S. M. O.; BRANDT, K.; GRAY, N. D.; WHITE, M. L.; MANNING, D. A. C. Comparison of silicate minerals as sources of potassium for plant nutrition in sandy soil. *European Journal of Soil Science*, v. 65, n. 5, p. 653-662, 2014.

MURAKAMI, T.; UTSUNOMIYA, S.; YOKOYAMA, T.; KASAMA, T. Biotite dissolution processes and mechanisms in the laboratory and in nature: early-stage weathering environment and vermiculitization. *American Mineralogist*, v. 88, n. 2-3, p. 377-386, 2003.

NAVARRO, G. R. B.; ZANARDO, A.; CONCEIÇÃO, F. T. Metamorphic evolution and P-T path of gneisses from Goiás magmatic arc in southwestern Goiás state. *Brazilian Journal of Geology*, v. 43, n. 2, p. 301-315, 2013.

NOROUZI, S.; KHADEMI, H. Ability of alfalfa (*Medicago sativa* L.) to take up potassium from different micaceous minerals and consequent vermiculitization. *Plant and Soil*, v. 328, n. 1, p. 83-93, 2010.

O'NEILL, M. E.; MATHEWS, K. A weighted least squares approach to Levene's test of homogeneity of variance. *Australian & New Zealand Journal of Statistics*, v. 42, n. 1, p. 81-100, 2000.

RYU, J.; VIGIER, N.; DECARREAU, A.; LEE, S.; LEE, K.; SONG, H.; PETIT, S. Experimental investigation of Mg isotope fractionation during mineral dissolution and clay formation. *Chemical Geology*, v. 445, n. 16, p. 135-145, 2016.

SANTOS, L. F.; SODRÉ, F. F.; MARTINS, S. M.; FIGUEIREDO, C. C.; BUSATO, J. G. Effects of biotite syenite on the nutrient levels and electrical charges in a Brazilian Savanna Ferralsol. *Pesquisa Agropecuária Tropical*, v. 51, e66691, 2021.

SCOTT, A. D.; AMONETTE, J. Role of iron in mica weathering. *In*: STUCKI, J. W.; GOODMAN, B. A.; SCHWERTMANN, U. (ed.). *Iron in soils and clay minerals*. Dordrecht: Springer, 1988.

SHAPIRO, S. S.; WILK, M. B. An analysis of variance test for normality (complete samples). *Biometrika*, v. 52, n. 3/4, p. 591-611, 1965.

THOMPSON, M. L.; UKRAINCZYK, L. Micas. *In*: DIXON, J. B.; SCHULZE, D. G. (ed.). *Soil mineralogy with environmental applications*. Madison: Soil Science Society of America, 2002.

TISCHENDORF, G.; FORSTER, H. J.; GOTTESMANN, B.; RIEDER, M. True and brittle micas: composition and solid-solution series. *Mineralogical Magazine*, v. 71, n. 3, p. 285-320, 2007.

WU, S.; LIU, Y.; SOUTHAM, G.; ROBERTSON, L. M.; WYKES, J.; YI, Q.; HALL, M.; LI, Z.; SUN, Q.; SAHA, N.; CHAN, T.; LU, Y.; HUANG, L. Rhizosphere drives biotite-like mineral weathering and secondary Fe-Si mineral formation in Fe ore tailings. *Earth and Space Chemistry*, v. 5, n. 3, p. 618-631, 2021.

YU, G. Root exudates and microbial communities drive mineral dissolution and the formation of nano-size minerals in soils: implications for soil carbon storage. *In*: GIRI, B.; PRASAD, R. A. V. (ed.). *Root biology*. Cham: Springer, 2018.